Supporting Information

Dual Rigid Donor and Acceptor Enabling Red Thermally Activated Delayed Fluorescence Emitters for Efficient OLEDs with Low Efficiency Roll-Off

Jinming Fan [a,b], Jingsheng Miao [a], Nengquan Li [a], Yitong Zeng [a], Changqing Ye [c], Xiaojun Yin [a,], and Chuluo Yang [a]*

[a] *Shenzhen Key Laboratory of New Information Display and Storage Materials, College of Materials Science and Engineering, Shenzhen University, Shenzhen 518060, People's Republic of China*

[b] *College of Physics and Optoelectronic Engineering, Shenzhen University, Shenzhen 518060, People's Republic of China*

[c] *Suzhou Key Laboratory of Flexible & Printing Optoelectronic Materials, School of Materials Science and Engineering, Suzhou University of Science and Technology, Suzhou, 215009, China*

Experimental Section

General information

^{1}H NMR and ^{13}C NMR spectra were recorded on Bruker AV 500 NMR spectrometer at room temperature using $CDCl_3$, DMSO-d_6 as solvent, and referenced externally to $SiMe_4$. The multiplicities of the signals are indicated as "*s*", "*d*", "*t*" or "*m*", which stand for singlet, doublet, triplet, and multiplet, respectively. High-resolution mass spectra (HRMS) were collected on a Bruker maxis UHR-TOF mass spectrometer in an APCI positive mode. Thermogravimetric analysis (TGA) was undertaken using a PerkinElmer Instruments (Pyris1 TGA) at a heating rate of 10 °C/ min from 30 to 800 °C under a nitrogen environment. The thermal decomposition temperatures (T_d) were determined by the recorded temperature at 5% weight loss. Differential scanning calorimetry (DSC) measurement was performed on DSC Q200 (TA instrument) with a heating rate of 10 °C min^{-1} from 25 to 450 °C under nitrogen. The glass transition temperature (T_g) was determined from the second heating scan. Cyclic voltammetry (CV) measurements were carried out on a CHI600 electrochemical analyzer (Chenhua, China) at room temperature, with a conventional three-electrode system consisting of a glassy carbon working electrode, a platinum wire auxiliary electrode, and an Ag/AgCl standard electrode was used as the reference electrode. The supporting electrolyte was 0.1 M tetrabutylammonium hexafluorophosphate (*n*-Bu_4NPF_6) in anhydrous dichloromethane solution, and ferrocene was added as an internal standard in the whole measurement. UV-Vis spectra in solution were recorded on a UV-3100 spectrophotometer at room temperature. Room-temperature photoluminescence spectra and phosphorescence spectra were measured on a Hitachi F-7000 fluorescence spectrophotometer with xenon lamp as the light source. The absolute fluorescence quantum yields (PLQY) were measured on a Quantaurus-QY measurement system (C9920-02, Hamamatsu Photonics) equipped with a calibrated integrating sphere. During the PLQY measurements, the integrating sphere was purged with pure and dry argon to maintain an inert environment. The lifetimes of fluorescence and delayed fluorescence were performed on PicoQuant Fluotime300.

Theoretical Calculations Method.

Density functional theory (DFT) calculations of the geometrical and electronic properties of the two emitters at ground-states or singlet states were performed based on the B3LYP/def2-SVP level including Grimme's dispersion correction, using Gaussian 16 software package. Time-dependent DFT (TD-DFT) calculations with PBE0 functional and def2-SVP basis set were then performed to further study the properties of excited states. All calculations were

performed in the gas phase, and visualized using GaussView 6.0. The calculation of root-mean-square deviations (RMSDs) between the optimized conformation of ground states and corresponding singlet states were analysed by VMD 1.9.3 program.

Analysis of Rate Constants:

The rate constants of radiative decay ($k_{r,s}$) and nonradiative decay ($k_{nr,s}$) from S_1 to S_0 states, the rate constants of intersystem crossing (k_{ISC}) and reverse intersystem crossing (k_{RISC}) were calculated from the following six equations:

$$k_p = 1/\tau_p \quad (1)$$

$$k_d = 1/\tau_d \quad (2)$$

$$k_{r,s} = \Phi_p k_p + \Phi_d k_d \approx \Phi_p k_p \quad (3)$$

$$k_{nr,s} = [(1-\Phi_{PL}) / \Phi_{PL}]\, k_{r,S} \quad (4)$$

$$k_{ISC} = k_p - k_{r,S} - k_{nr,S} \quad (5)$$

$$k_{RISC} = (k_p k_d \Phi_d)/(k_{ISC}\Phi_p) \quad (6)$$

Where τp and τd represent the prompt and decay fluorescence lifetime, which determined from transient PL spectra. The kp and kd represent the decay rate constants for prompt and delayed fluorescence, respectively. Φp and Φd indicate prompt and delayed fluorescence components and can be distinguished from the total ΦPL by comparing the integrated intensities of prompt and delayed components in the transient PL spectra.

Synthesis of Materials.

All reagents and chemicals (at least analytical grade) were purchased from commercial sources and used without further purification. Solvents were all dried and degassed using the Grubbs-type solvent purification system. The key intermediate of DP-TAT (**Scheme S1**) was prepared according to the previously literatures.[1,2]. Schlenk technology was strictly performed under argon conditions in all reactions. Air- and moisture-sensitive liquids and solutions were transferred via syringes. The final products were firstly purified by column chromatography, and then further refined by temperature-gradient vacuum sublimation.

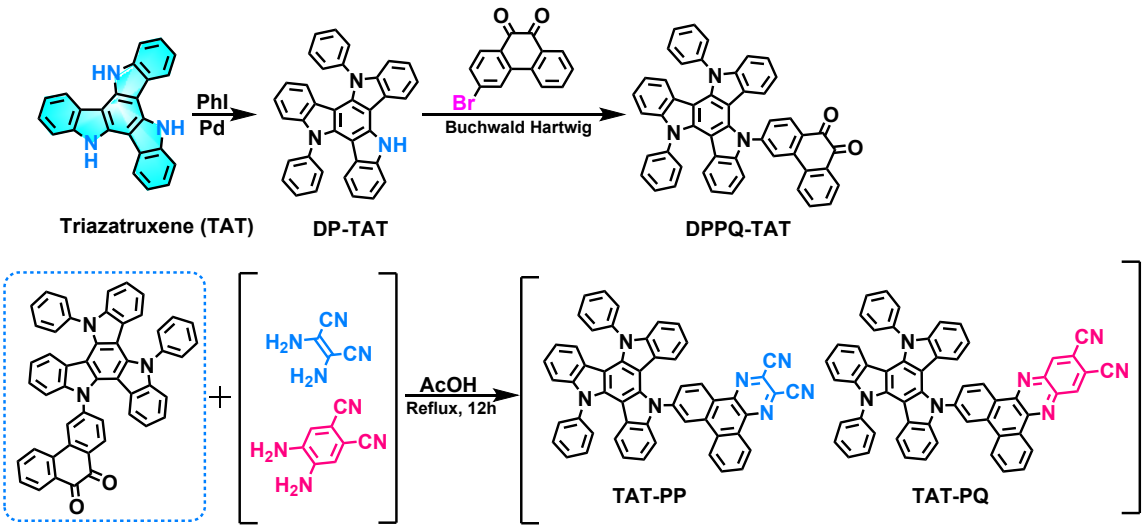

Scheme S1. Synthesis routes of the two red/deep-red TADF emitters.

General procedure for the synthesis of DPPQ-TAT.

The mixture of DP-TAT (1eq, 2 mmol, 0.99g), 3-Bromo-9,10-phenanthrenedione (1.5 eq, 3 mmol, 0.86g), $Pd_2(dba)_3$ (5 %, 0.1 mmol, 0.092 g), RuPhos (10 %, 0.2 mmol, 0.093 g) and Cs_2CO_3 (2 eq, 4 mmol, 1.3 g) was dissolved in a mixed solvent composed of dry toluene (40 ml). The reaction mixture was allowed to stir at 110 °C for 24 h under Ar. Then the reaction mixture was cooled at room temperature and filtered through Celite. Filtrate was concentrated under reduced pressure, the residue was dissolved in CH_2Cl_2 (40 mL × 3), washed with water and dried over Na_2SO_4. Combined organic layers were evaporated under reduced pressure, and the residue was purified by column chromatography on silica [DCM/Hex = (1/1) ~DCM] to provide pure **DPPQ-TAT**.

General procedure for the synthesis of TAT-PP and TAT-PQ.

Under argon atmosphere, to a 50 mL round-bottom flask equipped with magnetic stirring bar and reflux condenser, **DPPQ-TAT** (1eq, 2 mmol, 1.4 g), corresponding diamino compound (2,3-diaminomaleonitrile, 4,5-diaminophthalonitrile) (1.1 eq, 2.2 mmol) and acetic acid glacial (20 mL) were added. The mixture was stirred at 120 °C for 24 h, then cooled down to room temperature. Then, the mixture was poured into the water and extracted with DCM (20 mL × 3). The combined organic layers were dried over Na_2SO_4 and concentrated under reduced pressure. and the deep red solid was collected by filtration. Column chromatography on silica [DCM/Hex = (1/1) ~DCM] to provide pure **TAT-PP, TAT-PQ**.

NMR Data:

5,10-Diphenyl-10,15-dihydro-5*H*-diindolo[3,2-a:3',2'-c]carbazole (DP-TAT)

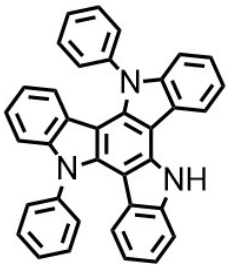

Yield: 53% (1.8 g). White solid. ^{1}H NMR (500 MHz, DMSO-d_6) δ 12.01 (s, 1H), 8.88 (d, J = 7.7 Hz, 1H), 7.88 – 7.57 (m, 11H), 7.49 (ddd, J = 7.9, 6.5, 1.7 Hz, 1H), 7.42 (qd, J = 8.1, 1.4 Hz, 2H), 7.29 – 7.16 (m, 2H), 7.16 – 7.10 (m, 1H), 6.72 (ddd, J = 8.1, 6.8, 1.2 Hz, 1H), 6.66 (ddd, J = 8.2, 7.0, 1.1 Hz, 1H), 5.97 (d, J = 8.1 Hz, 1H), 5.78 (s, 1H). [1-2]

3-(10,15-Diphenyl-10,15-dihydro-5*H*-diindolo[3,2-a:3',2'-c]carbazol-5-yl)phenanthrene-9,10-dione (DPPQ-TAT):

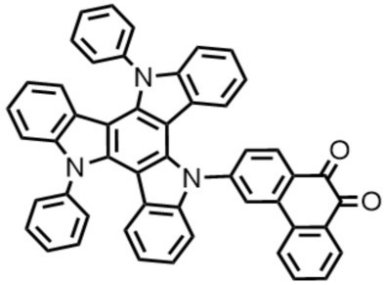

Yield: 75% (1.05 g). Dark-purple solid. ^{1}H NMR (500 MHz, DMSO-d_6) δ 8.84 (d, J = 2.0 Hz, 1H), 8.42 – 8.37 (m, 1H), 8.25 (d, J = 8.2 Hz, 1H), 8.12 (dd, J = 7.8, 1.5 Hz, 1H), 7.79 – 7.68 (m, 11H), 7.64 (dd, J = 8.2, 1.9 Hz, 1H), 7.57 (td, J = 7.6, 1.0 Hz, 1H), 7.50 (d, J = 8.2 Hz, 1H), 7.29 (t, J = 7.7 Hz, 2H), 7.26 – 7.16 (m, 3H), 6.87 (ddd, J = 8.2, 7.0, 1.1 Hz, 1H), 6.77 (dddd, J = 16.5, 8.2, 7.0, 1.1 Hz, 2H), 6.49 (d, J = 8.1 Hz, 1H), 6.06 – 5.98 (m, 2H). ^{13}C NMR (126 MHz, DMSO-d_6) δ 178.19, 146.14, 141.30, 140.63, 140.05, 137.43, 137.13, 136.92, 136.39, 135.48, 131.70, 131.40, 130.49, 130.30, 129.94, 129.24, 128.72, 128.57, 128.43, 125.23, 123.85, 123.76, 123.73, 123.69, 122.07, 121.43, 120.69, 120.58, 120.15, 110.15, 110.05, 109.98, 104.49, 104.35, 104.01. HRMS (APCI) m/z calcd for. $C_{50}H_{29}N_3O_2$ $[M+H]^+$ 704.2333, found 704.2333. Elemental analysis (%) calcd for $C_{50}H_{29}N_3O_2$: C 85.33, H 4.15, N 5.97; found: C 84.75, H 4.39, N 5.63.

7-(10,15-Diphenyl-10,15-dihydro-5H-diindolo[3,2-a:3',2'-c]carbazol-5-yl)dibenzo[*f*,*h*]quinoxaline-2,3-dicarbonitrile (TAT-PP):

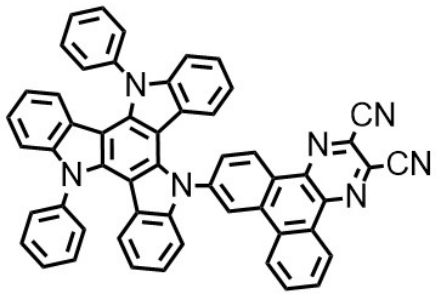

Yield: 52 % (0.81 g). Dark-red solid. ^{1}H NMR (500 MHz, Chloroform-*d*) δ 9.29 (d, J = 8.5 Hz, 1H), 9.04 (dd, J = 8.1, 1.4 Hz, 1H), 8.88 (d, J = 2.0 Hz, 1H), 8.42 (d, J = 8.2 Hz, 1H), 7.98 (dd, J = 8.7, 1.9 Hz, 1H), 7.80 – 7.76 (m, 1H), 7.68 (dtd, J = 13.5, 6.0, 4.0 Hz, 11H), 7.59 (d, J = 8.2 Hz, 1H), 7.36 (d, J = 8.2 Hz, 1H), 7.26 (d, J = 6.4 Hz, 1H), 7.24 – 7.19 (m, 2H), 6.96 (t, J = 7.6 Hz, 1H), 6.85 (t, J = 7.6 Hz, 1H), 6.80 (t, J = 7.6 Hz, 1H), 6.39 (t, J = 7.6 Hz, 1H), 6.15 – 6.05 (m, 3H). ^{13}C NMR (126 MHz, Chloroform-*d*) δ

145.10, 142.85, 142.28, 141.82, 141.27, 140.85, 140.71, 136.91, 134.65, 132.87, 132.58, 130.33, 130.18, 129.43, 129.10, 129.06, 128.55, 127.74, 127.12, 126.06, 123.75, 123.68, 123.53, 123.49, 123.37, 123.09, 122.81, 122.31, 122.03, 122.00, 121.87, 121.18, 120.34, 119.99, 113.83, 110.21, 110.12, 109.65, 105.50. HRMS (APCI) m/z calcd for. $C_{54}H_{29}N_7$ $[M+H]^+$ 776.2558, found 776.2556. Elemental analysis (%) calcd for $C_{54}H_{29}N_7$: C 83.60, H 3.77, N 12.64; found: C 84.29, H 3.98, N 12.67.

3-(10,15-Diphenyl-10,15-dihydro-5H-diindolo[3,2-a:3',2'-c]carbazol-5-yl)dibenzo[*a*,*c*]phenazine-11,12-dicarbonitrile (TAT-PQ):

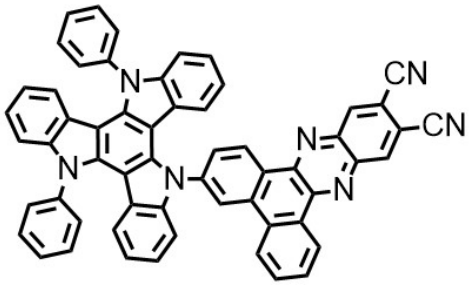

Yield: 54 % (0.89 g). Dark-green solid. ^{1}H NMR (500 MHz, Chloroform-*d*) δ 9.44 (d, *J* = 8.4 Hz, 1H), 9.23 (dd, *J* = 8.0, 1.5 Hz, 1H), 8.85 (d, *J* = 2.0 Hz, 1H), 8.60 (d, *J* = 13.8 Hz, 2H), 8.40 (d, *J* = 8.1 Hz, 1H), 7.93 (dd, *J* = 8.5, 1.9 Hz, 1H), 7.79 – 7.75 (m, 1H), 7.74 – 7.63 (m, 11H), 7.59 (d, *J* = 8.2 Hz, 1H), 7.34 (d, *J* = 8.2 Hz, 1H), 7.24 – 7.17 (m, 3H), 6.91 (t, *J* = 7.6 Hz, 1H), 6.83 (t, *J* = 7.6 Hz, 1H), 6.81 – 6.76 (m, 1H), 6.43 (t, *J* = 7.7 Hz, 1H), 6.26 (d, *J* = 8.2 Hz, 1H), 6.09 (d, *J* = 8.2 Hz, 1H), 6.04 (d, *J* = 8.1 Hz, 1H). ^{13}C NMR (126 MHz, Chloroform-*d*) δ 145.80, 145.25, 144.78, 141.99, 141.99, 141.81, 141.79, 141.39, 140.78, 137.77, 137.52, 137.25, 137.20, 137.04, 132.58, 132.46, 130.18, 129.42, 129.32, 129.25, 129.10, 129.03, 128.55, 128.33, 127.89, 127.34, 123.72, 123.66, 123.33, 123.05, 122.76, 122.41, 122.14, 122.13, 121.03, 120.35, 120.12, 115.34, 115.33, 113.41, 113.41, 113.37, 110.16, 110.09, 109.77, 105.36. HRMS (APCI) m/z calcd for. $C_{58}H_{31}N_7$ $[M+H]^+$ 826.2714, found 826.2718. Elemental analysis (%) calcd for $C_{58}H_{31}N_7$: C 84.35, H 3.78, N 11.87; found: C 84.63, H 3.97, N 11.68.

References

[1] K. J. Kim, G. H. Kim, R. Lampande, D. H. Ahn, J. B. Im, J. S. Moon, J. K. Lee, J. Y. Lee, J. Y. Lee, J. H. Kwon, *J. Mater. Chem. C* 2018, **6**, 1343-1348.

[2] Y. Chen, S. Wang, X. Wu, Y. Xu, H. Li, Y. Liu, H. Tong, L. Wang, *J. Mater. Chem. C* 2018, **6**, 12503-12508.

NMR and HRMS

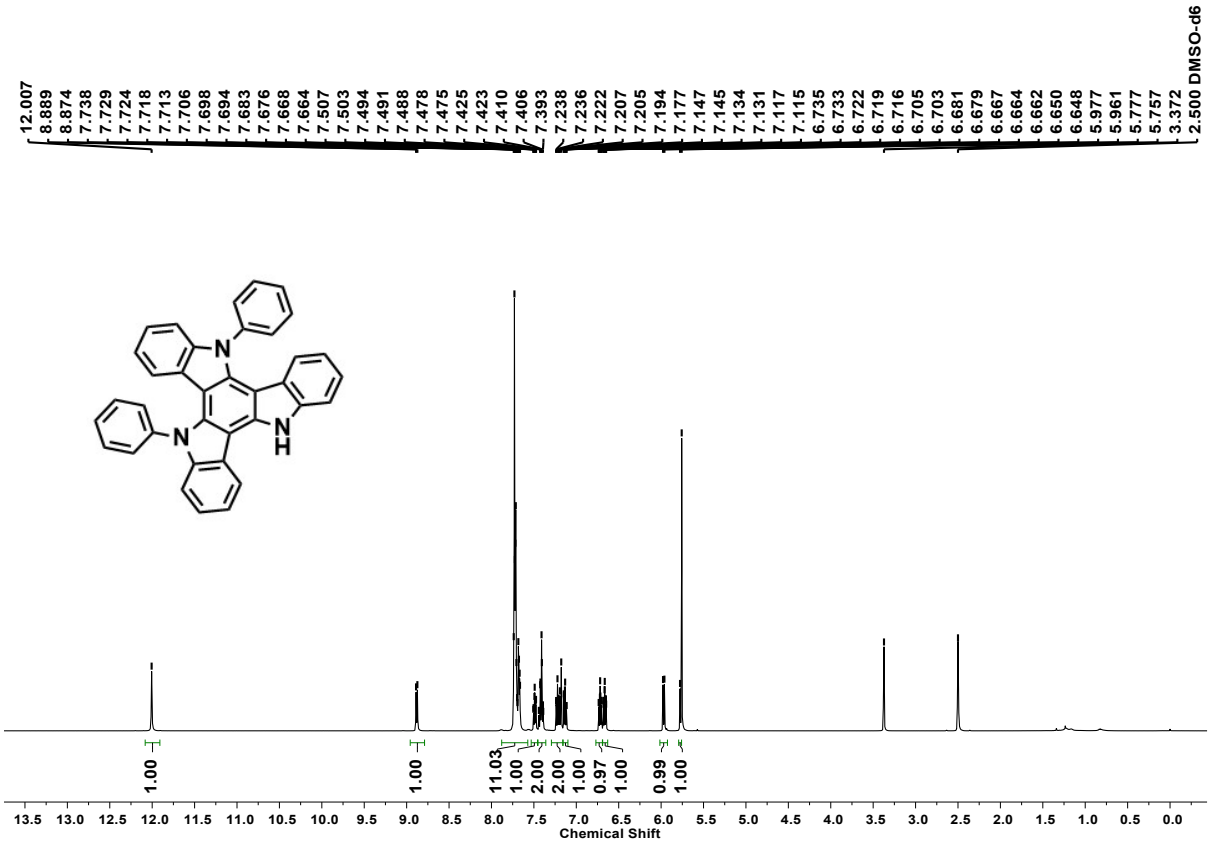

Fig. S1. ^{1}H NMR of **DP-TAT** in DMSO-d_6.

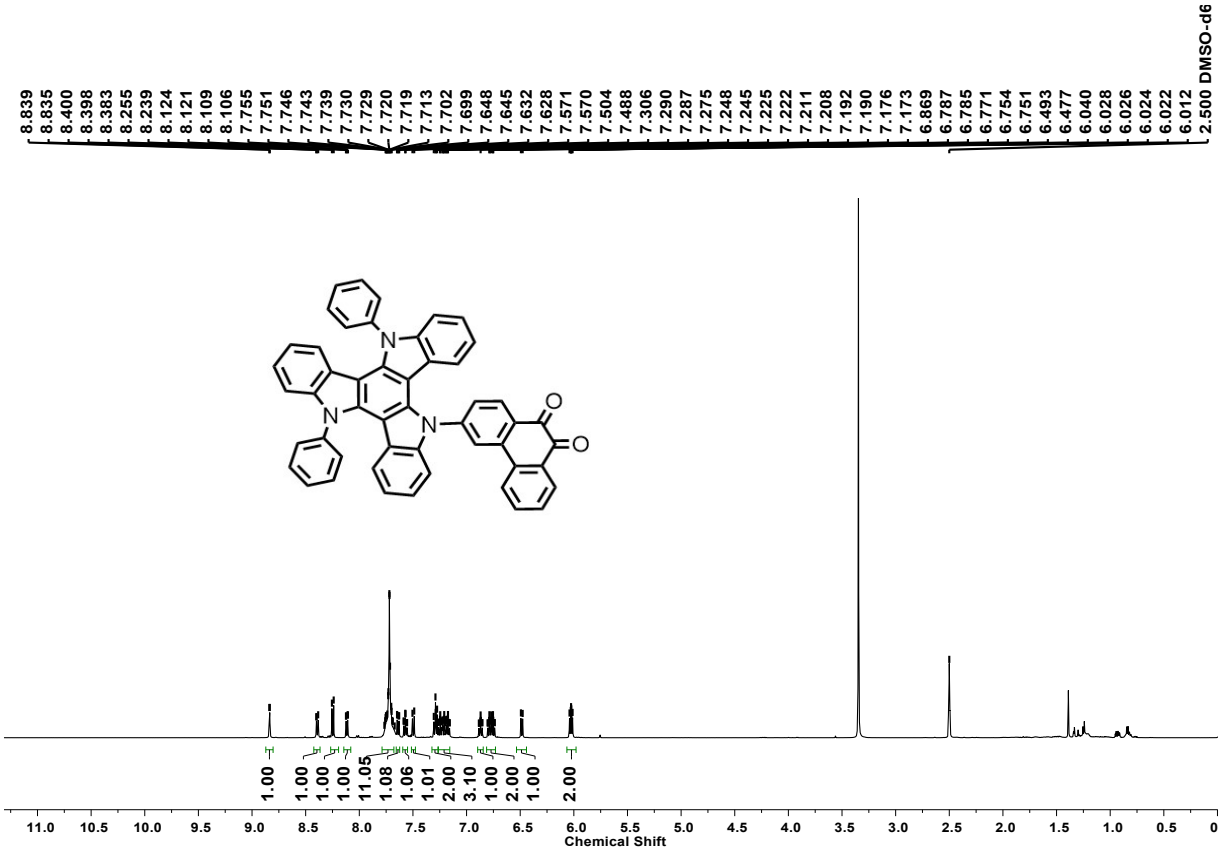

Fig. S2. [1]H NMR of **DPPQ-TAT** in DMSO-d_6.

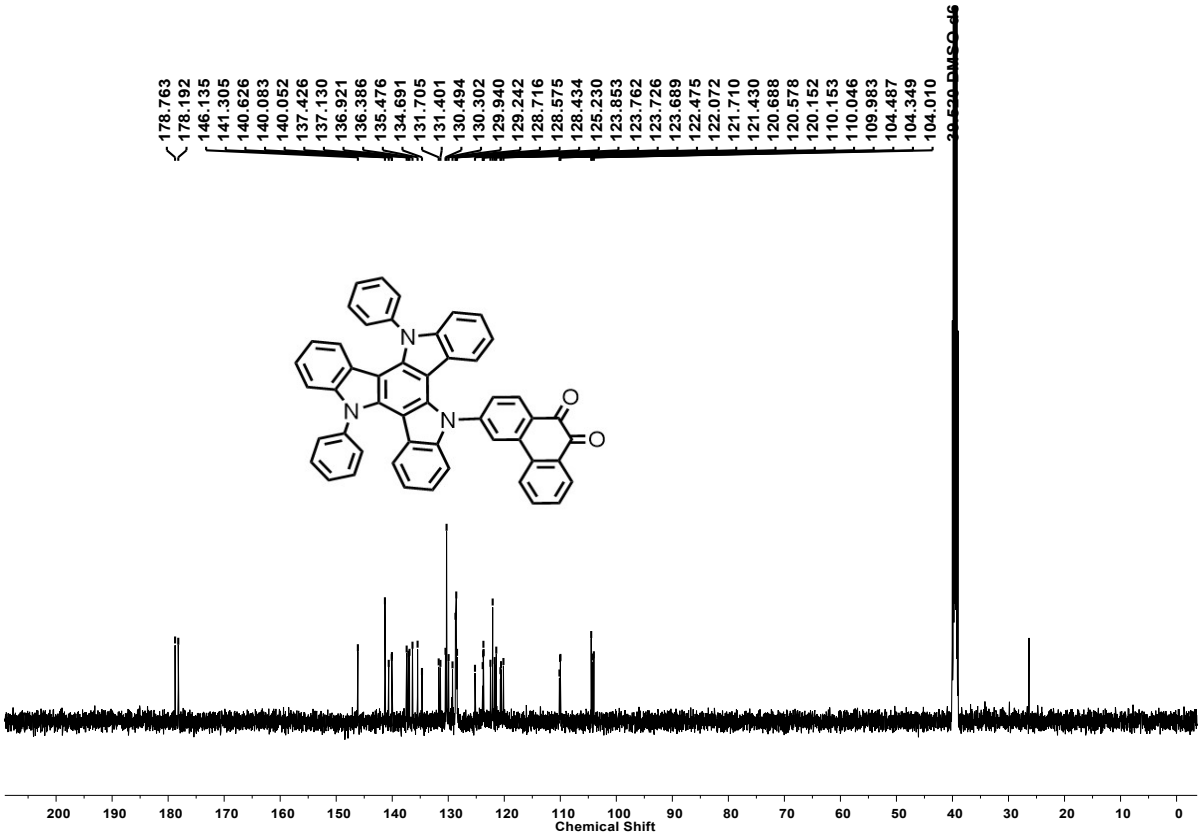

Fig. S3. [13]C NMR of **DPPQ-TAT** in DMSO-d_6

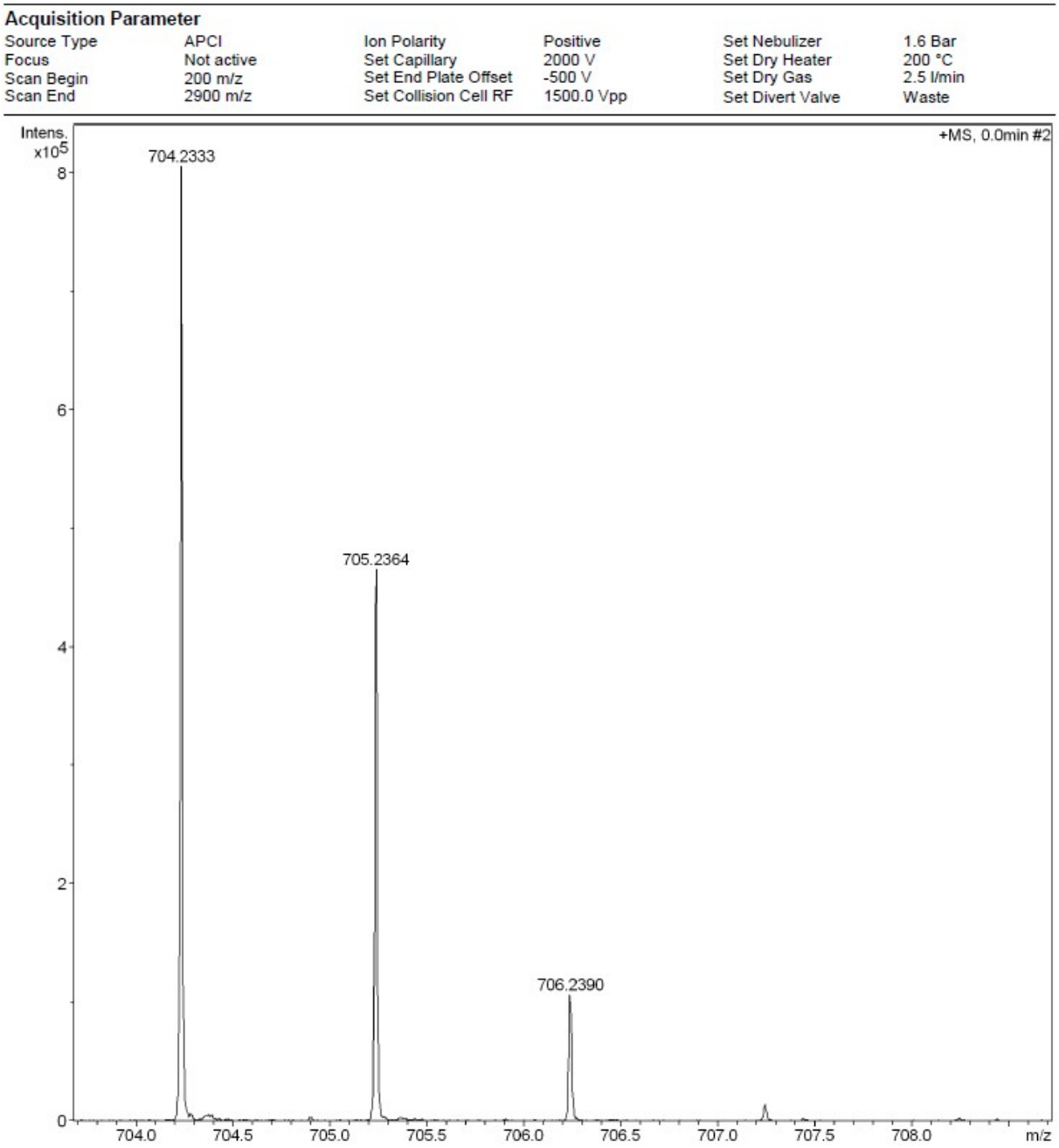

Fig. S4. HRMS (APCI) of **DPPQ-TAT** in MeOH.

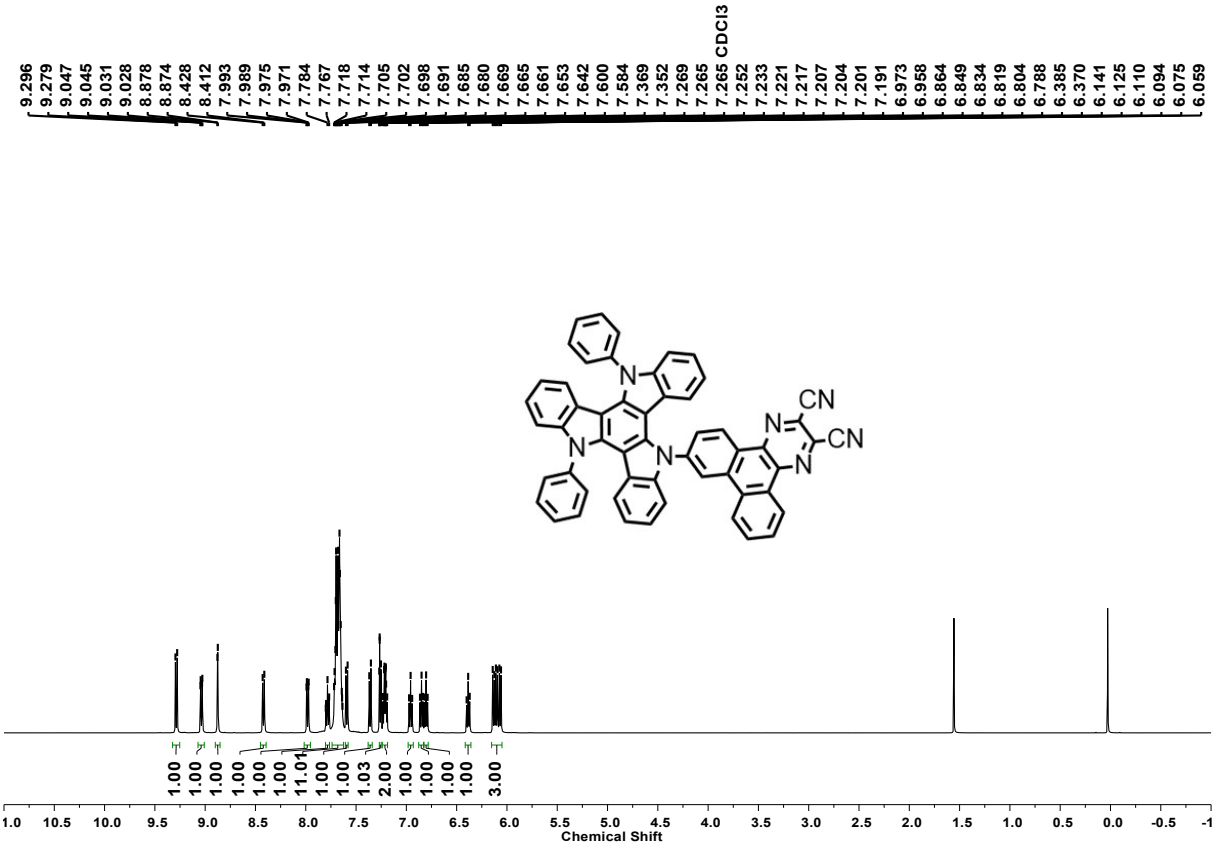

Fig. S5. ^{1}H NMR of **TAT-PP** in $CDCl_3$.

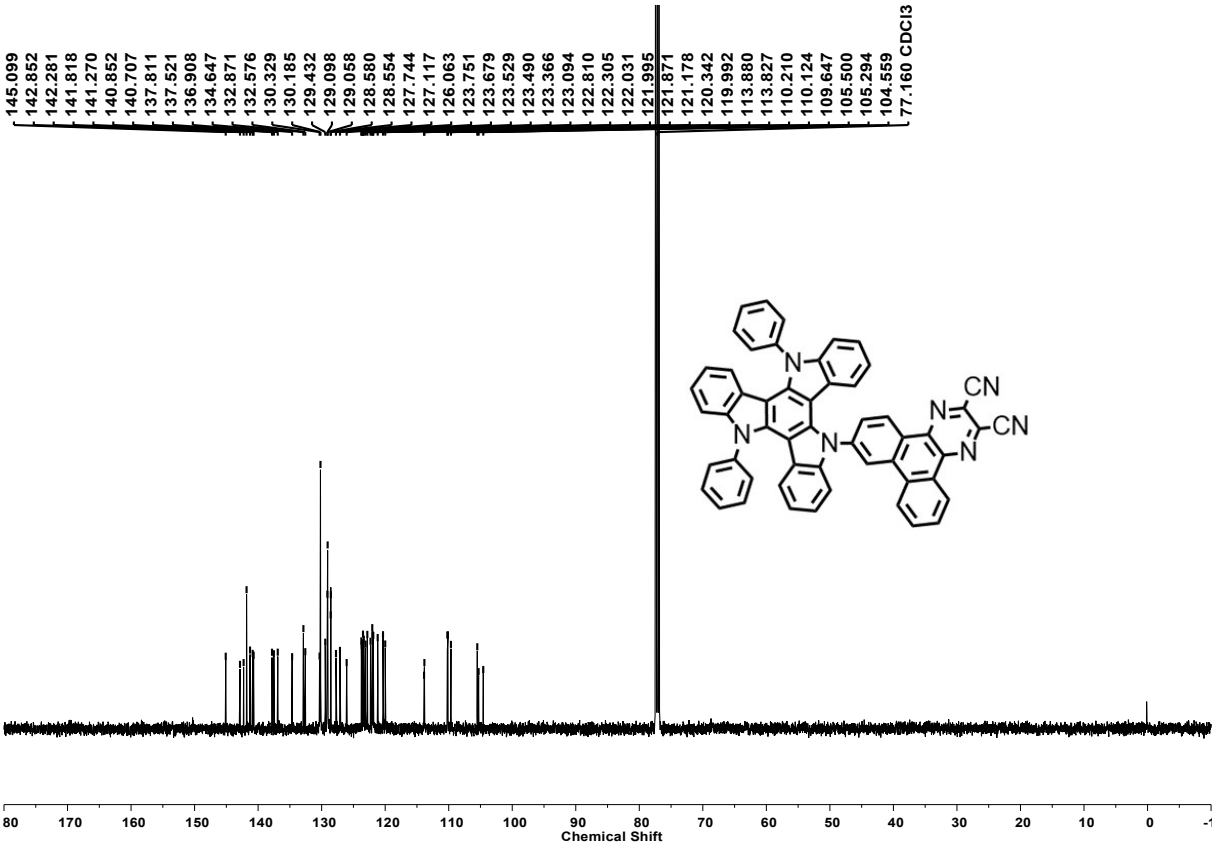

Fig. S6. ^{13}C NMR of **TAT-PP** in $CDCl_3$.

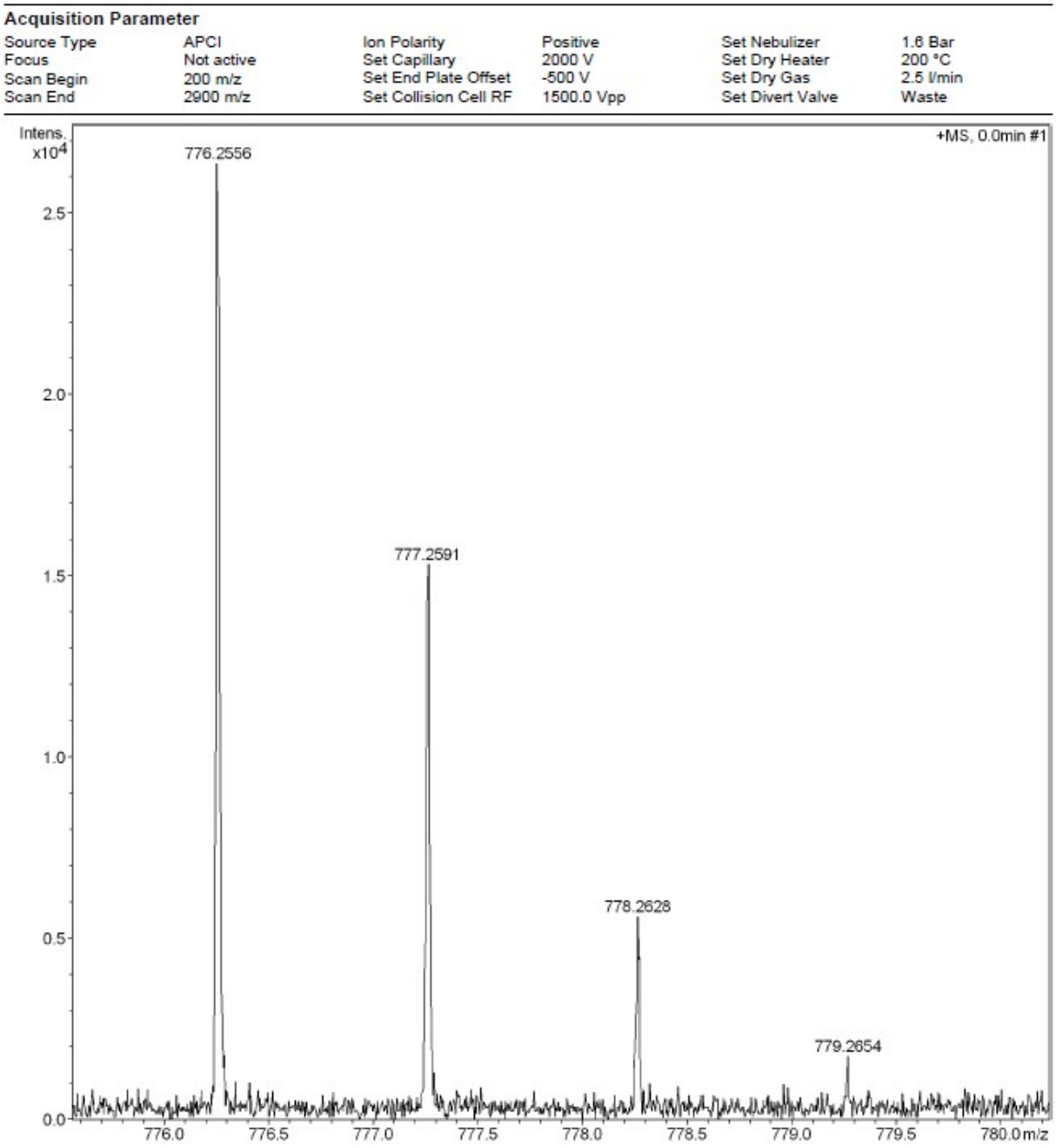

Fig. S7. HRMS (APCI) of **TAT-PP** in MeOH.

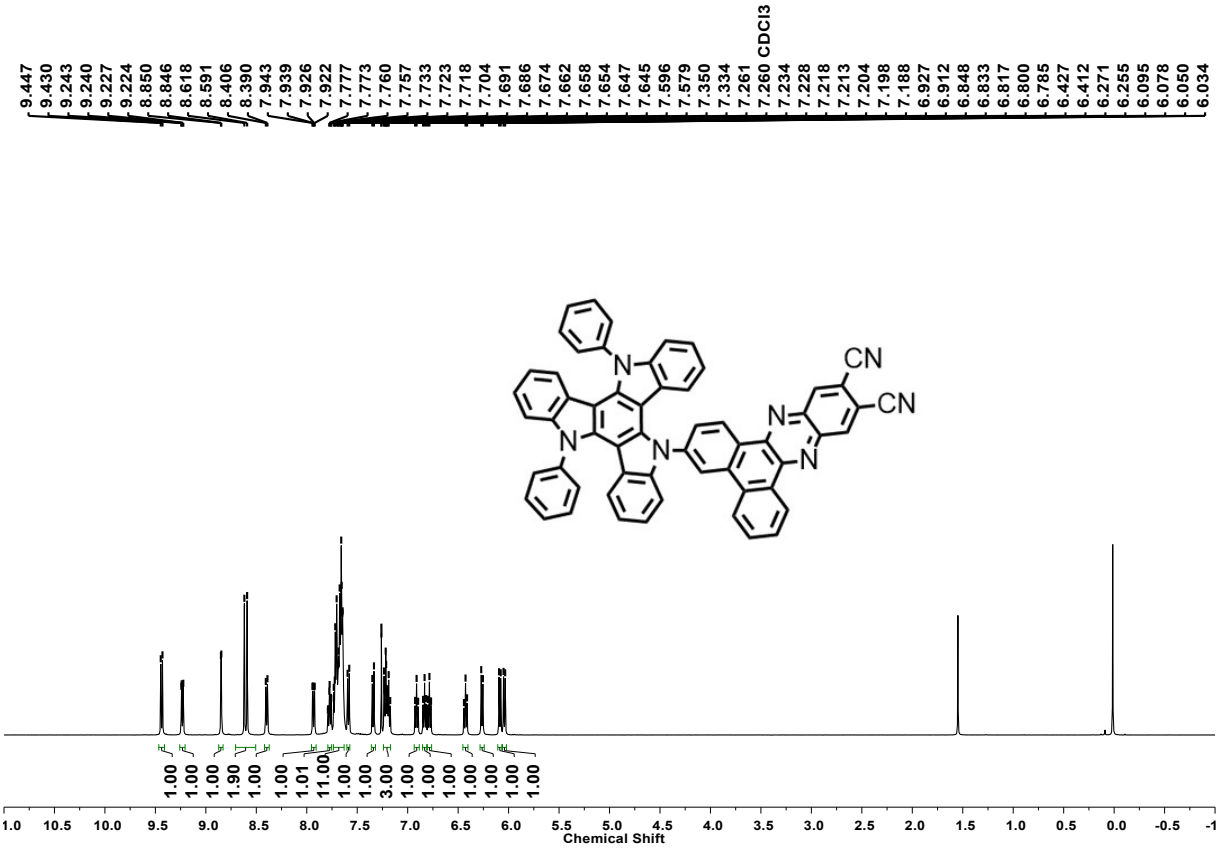

Fig. S8. ^{1}H NMR of **TAT-PQ** in $CDCl_3$.

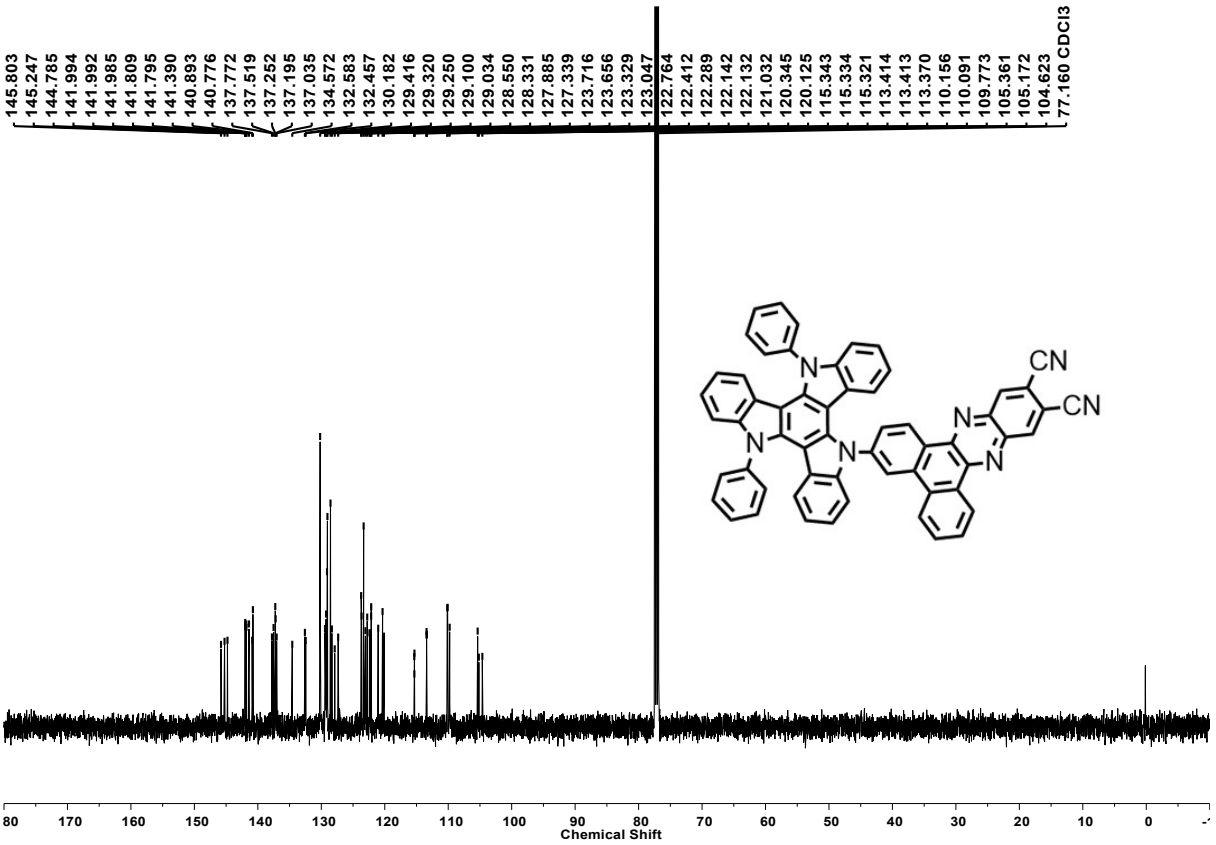

Fig. S9. ^{13}C NMR of **TAT-PQ** in $CDCl_3$.

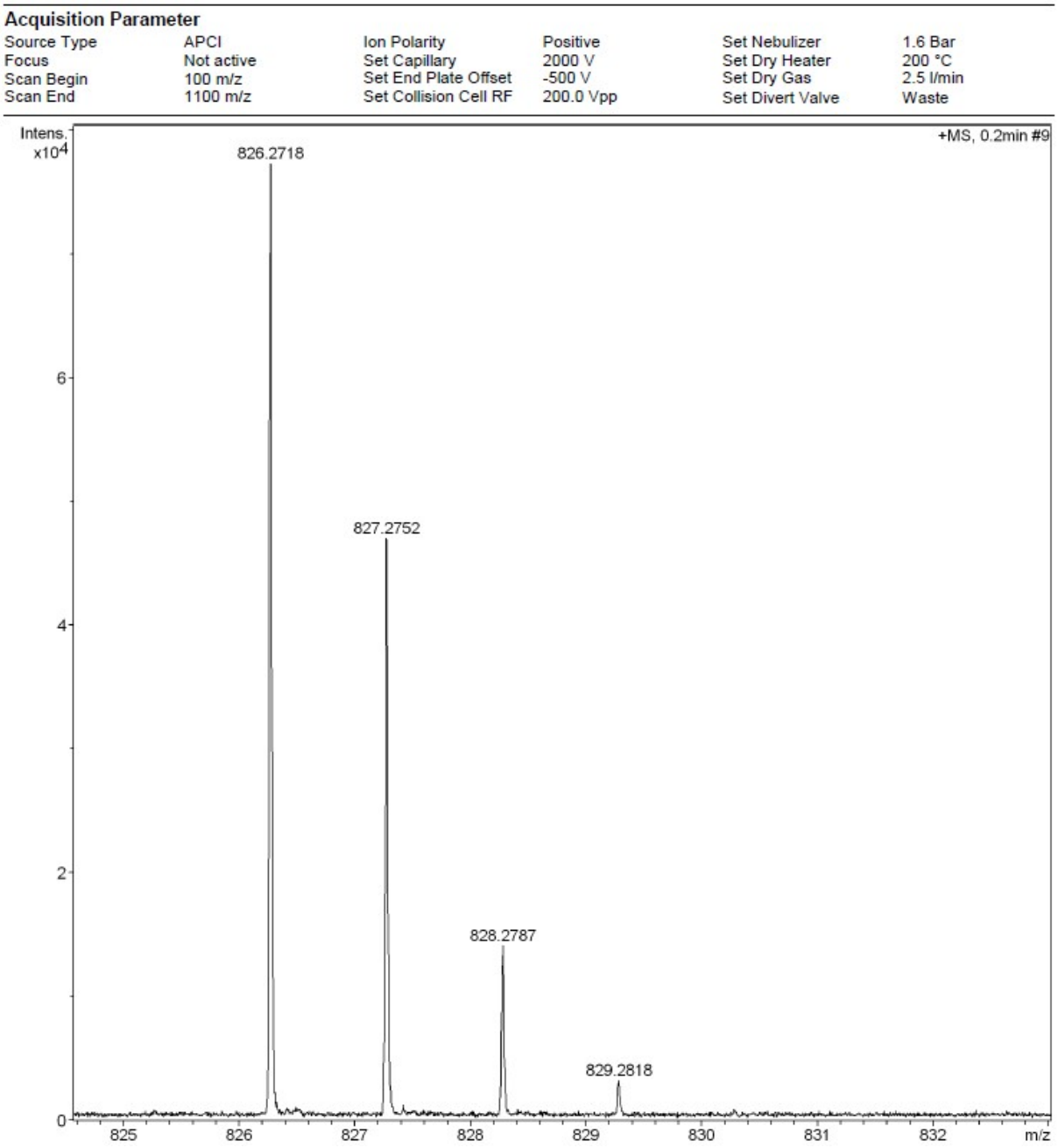

Fig. S10. HRMS (APCI) of **TAT-PQ** in MeOH.

Table S1, Crystal data for **TAT-PP**.

Identification code	47-0m-sq
Empirical formula	$C_{56}H_{33}Cl_4N_7$
CCDC No.	2123959
Formula weight	945.69
Temperature/K	170.0
Crystal system	triclinic
Space group	P-1
a/Å	13.809(4)
b/Å	18.949(5)
c/Å	19.274(5)
α/°	100.295(8)
β/°	101.906(9)
γ/°	102.245(8)
Volume/Å^3	4690(2)
Z	4
ρ_{calc}g/cm^3	1.339
μ/mm^{-1}	0.300
F(000)	1944.0
Crystal size/mm^3	0.16 × 0.12 × 0.11
Radiation	MoKα (λ = 0.71073)
2Θ range for data collection/°	3.866 to 53.008
Index ranges	$-17 \leq h \leq 17$, $-23 \leq k \leq 22$, $-24 \leq l \leq 23$
Reflections collected	53639
Independent reflections	19020 [R_{int} = 0.0939, R_{sigma} = 0.1155]
Data/restraints/parameters	19020/0/1207
Goodness-of-fit on F^2	1.038
Final R indexes [I>=2σ (I)]	R_1 = 0.0805, wR_2 = 0.2005
Final R indexes [all data]	R_1 = 0.1579, wR_2 = 0.2498
Largest diff. peak/hole / e Å^{-3}	1.05/-0.95

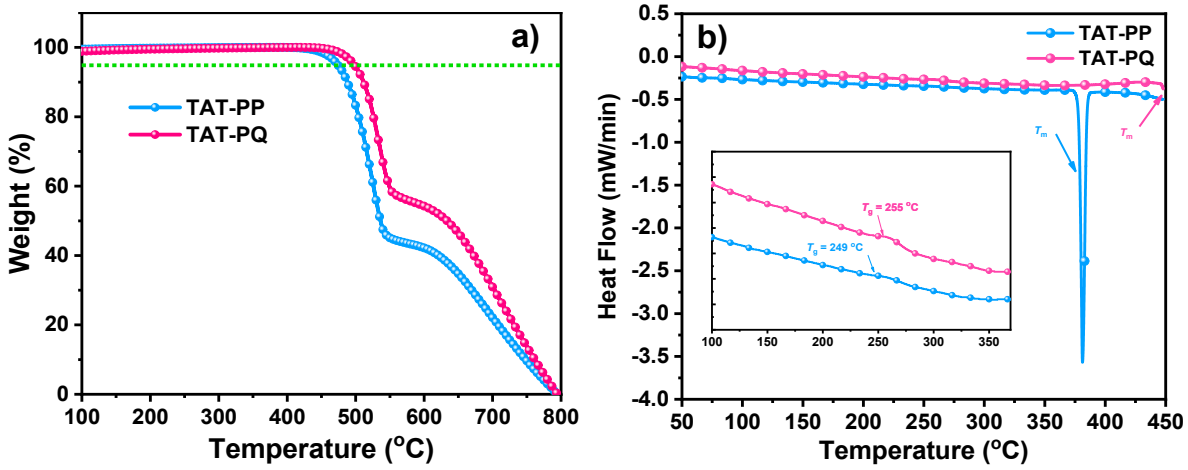

Fig. S11. The TGA and DSC curves of **TAT-PP** and **TAT-PQ**.

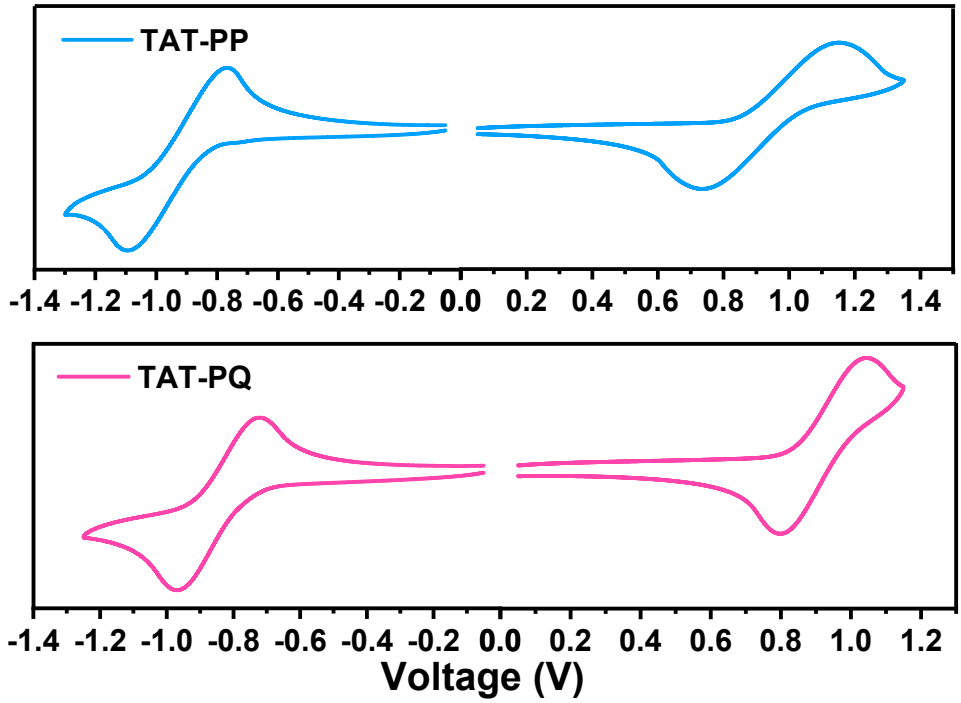

Fig. S12. Cyclic voltammetry analysis of **TAT-PP** and **TAT-PQ**.

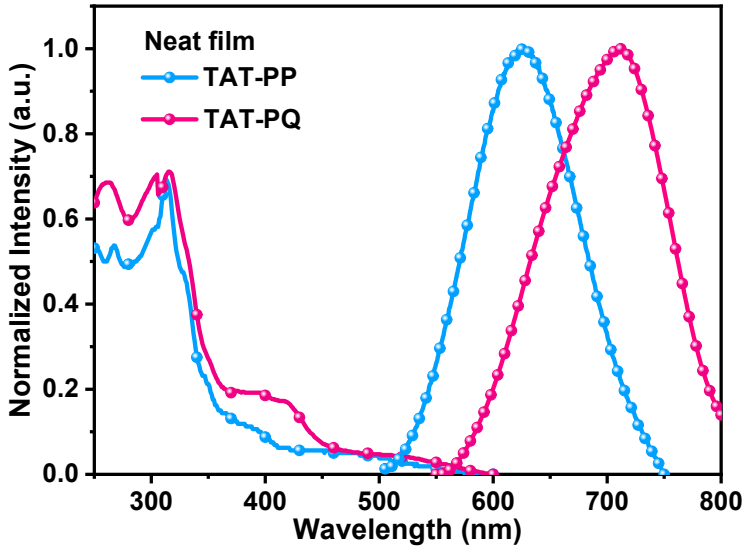

Fig. S13. UV-vis absorption and photoluminescence (PL) spectra of the **TAT-PP** and **TAT-PQ** in neat films, obviously deep-red/NIR emission peaks of 634 and 721 nm can be observed on **TAT-PP** and **TAT-PQ**.

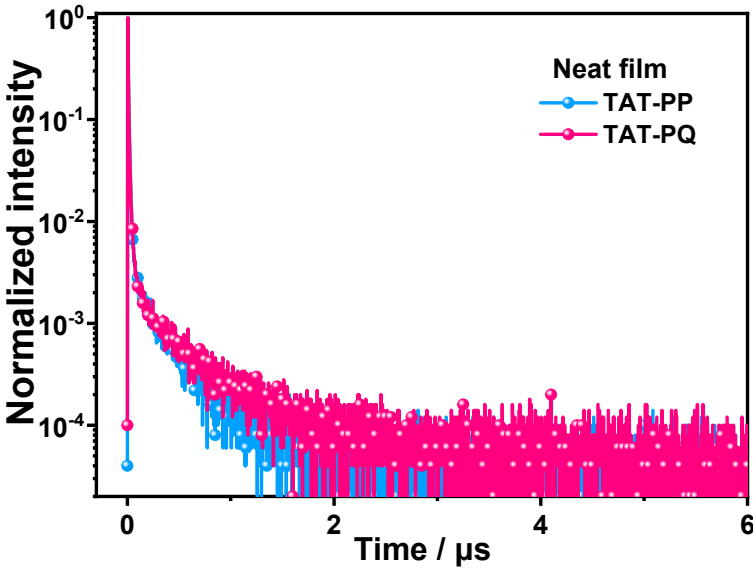

Fig. S14. Transient PL decay curves of **TAT-PP** and **TAT-PQ** in neat film under argon atmosphere, two films exhibited a second-order exponential PL decays.

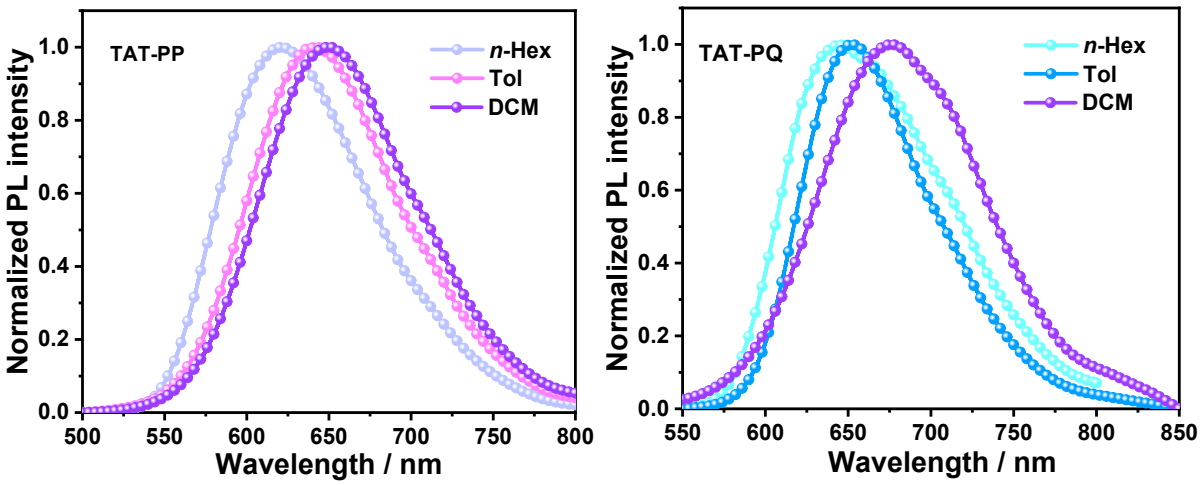

Fig. S15. Normalized PL spectrum of **TAT-PP** and **TAT-PQ** in different polarity solvents (10^{-5} mol/L).

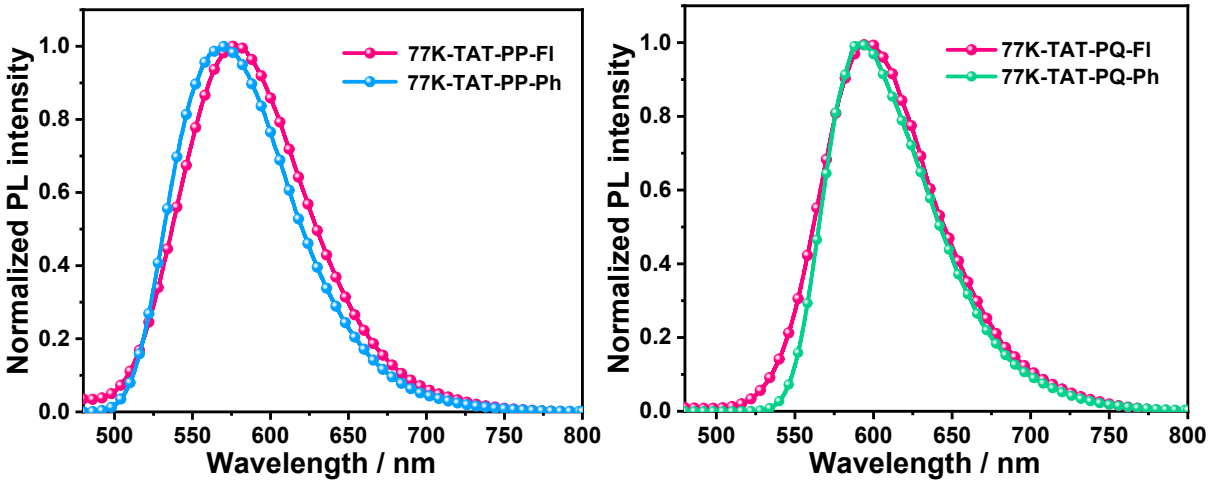

Fig. S16. Low-temperature photoluminescence LTPL (77K) spectra of doped film with 1 wt.% **TAT-PP** or **TAT-PQ** in 2, 6-DCzPPy host. The onset energy of LTPL spectra were used to determine the S_1 and T_1 energy level, 2.43/2.42 eV for TAT-PP and 2.30/2.28 eV for TAT-PQ, respectively. The corresponding ΔE_{ST} was measured to be 0.01 eV and 0.02 eV.

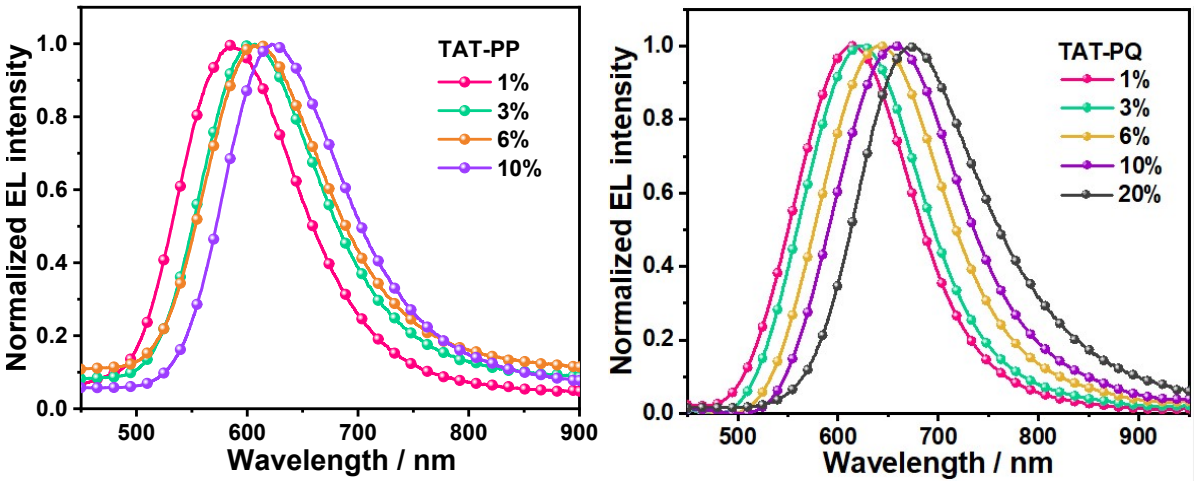

Fig. S17. TAT-PP and **TAT-PQ** exhibited increase of doping concentrations from 1 to 10%, red-shifted EL spectra were recorded for all three emitters by strong intermolecular interaction. Among them, high concentration doping (20%) was tested for **TAT-PQ**, and the maximum emission peak position of the EL spectrum was at 678nm.

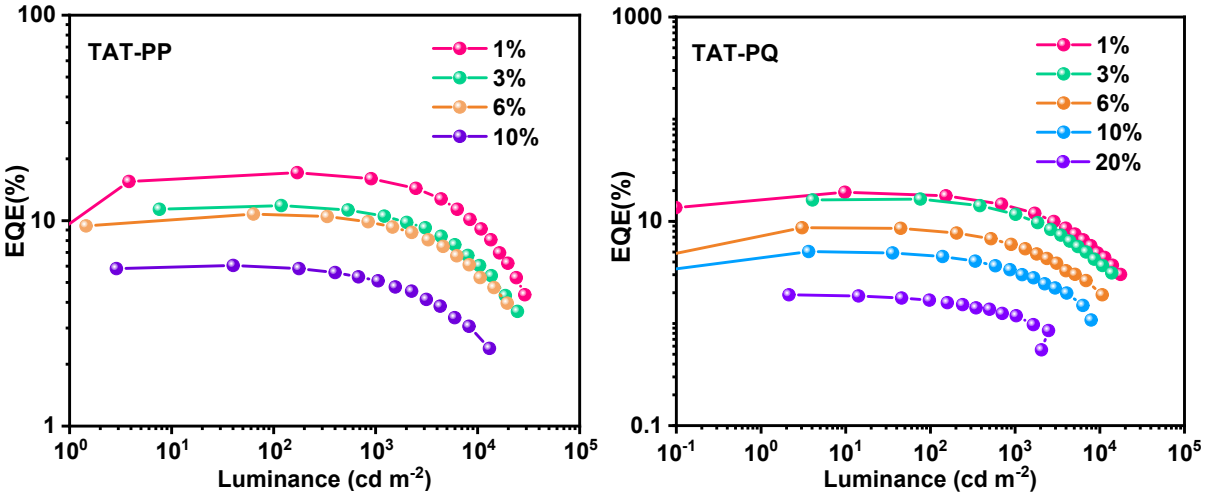

Fig. S18. TAT-PP and **TAT-PQ** emitters exhibited maximum EQE values at a low doping concentration of 1 wt.%, and further increase of doping concentrations from 1 to 10 % decreased the maximum EQE values, due to the concentration quenching effect.

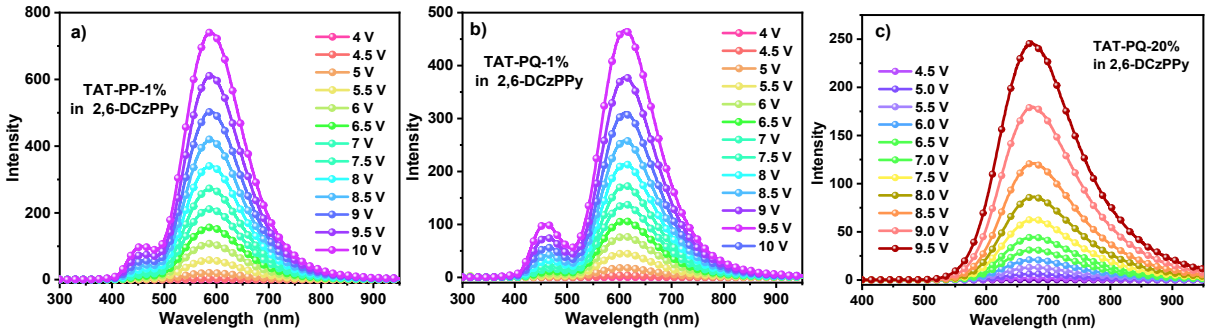

Fig. S19. The EL spectra of device a) A, b) B and c) C under different driving voltages, respectively.

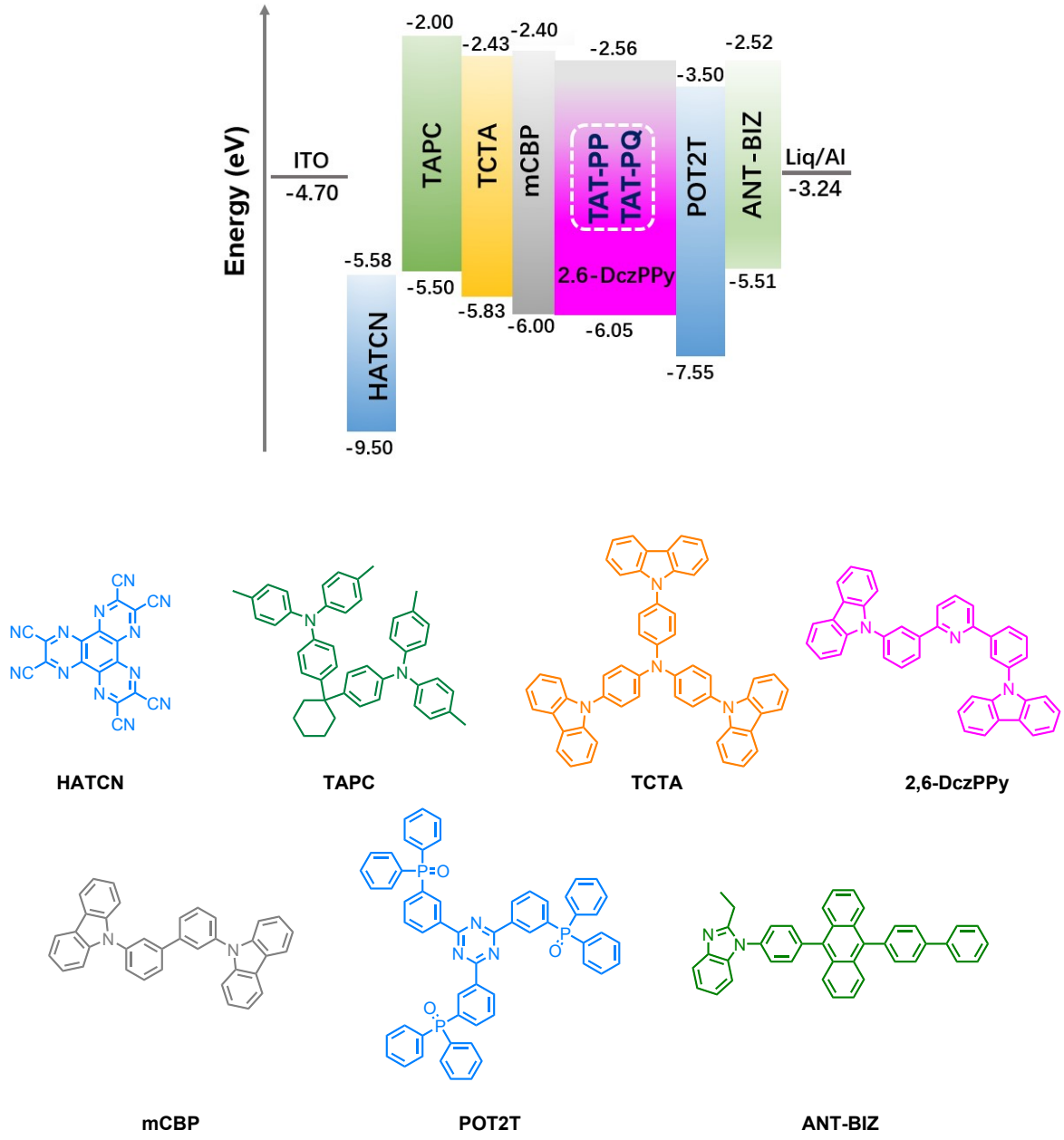

Fig. S20. Chemical structures of the used materials.